Supplementary Information

Free Tropospheric Aerosols at the Mt. Bachelor Observatory: More Oxidized and Higher Sulfate Content Compared to Boundary Layer Aerosols

Shan Zhou[1], Sonya Collier[1], Daniel A. Jaffe[2,3], Qi Zhang[1*]

[1]Department of Environmental Toxicology, University of California, Davis, CA 95616, USA
[2]School of Science, Technology, Engineering, and Mathematics, University of Washington Bothell, Bothell, WA, USA
[3]Department of Atmospheric Sciences, University of Washington, Seattle, WA, USA

Correspondence to: Qi Zhang (dkwzhang@ucdavis.edu)

Section 1. Distinguish Free Tropospheric Air from Boundary Layer-Influenced Air

Extensive work has been done at MBO to differentiate free troposphere air (FT) from boundary layer (BL)-influenced air. Several water vapor ($H_2O_{(g)}$) mixing ratio-based segregation techniques have been used to date. Weiss-Penzias et al. (2006) and Fischer et al. (2010) used percentiles of water vapor mixing ratio to identify FT and BL-influences air masses. These same studies also used water vapor calculated from the 0 and 12 UTC National Weather Service soundings from Medford, Oregon and Salem, Oregon to determine a representative altitude for the air masses sampled at MBO. Reidmiller et al. (2010) used chairlift soundings of water vapor mixing ratios at Mt. Bachelor coupled with high-resolution NO_x data from MBO to determine a time of day when the BL influence began at the mountain summit. While all these studies focus on segregating FT and BL-influenced air masses during Spring, Ambrose et al. (2011) used sounding data from Medford to compare with $H_2O_{(g)}$ distributions at MBO and obtained a seasonal mean $H_2O_{(g)}$ mixing ratios for MBO FT data, which for winter, spring, summer, and fall seasons corresponded with WV < 3.28, < 3.28, <5.4, and <4.12 g kg^{-1}. Based on the same work by Ambrose et al. (2011), McClure et al. (2016) interpolated between the seasonal values into a monthly criterion. Zhang and Jaffe (2017) contributed to a more accurate monthly FT/BL-influence isolation at MBO based on comparison of MBO $H_2O_{(g)}$ distributions to the $H_2O_{(g)}$ soundings from Medford and Salem, Oregon, at equivalent pressure level. $H_2O_{(g)}$ criteria for FT air masses at MBO were referred to the cut points when equivalent monthly averages of the retained drier portion of the MBO data and the soundings were obtained. The FT/BL-influenced water vapor criterion for each month is 3.26, 2.64, 2.46, 2.55, 3.06, 4.25, 5.14, 5.23, 4.60, 4.36, 3.44, 2.97 (from January to December).

Venzac et al. (2009) derived the boundary layer height of the puy de Dome using the ECMWF IFS model. Model results showed that the site (1465 a.s.l.) lied above the BL all times in winter while in summer it was strongly influenced by BL during the day but was above the BL at night. Collaud Coen et al. (2011) estimated BL influence at the Jungfraujoch research site (JFJ; 3580 a.s.l) by classifying daily synoptic weather situations and concluded that JFJ was largely influenced by the BL at night in summer during the subsidence weather type.

We derived the BL height at MBO during the study period based on the HYSPLIT model using the 40 km resolution US Eta Data Assimilation System (EDAS) meteorological data. The $H_2O_{(g)}$ mixing ratio at MBO showed a clear average diurnal variation similar to that of the BL height (Fig. 2). This suggest that it is valid to use $H_2O_{(g)}$ mixing ratio to distinguish FL and BL-influenced air masses in this study. Comparing to the estimated BL height, measured $H_2O_{(g)}$ mixing ratio provide more details in its temporal variations. For example, as seen in Fig. S14, from the evening of 7/25 to the morning of 7/26, the estimated mixing depth at MBO was below 300 m which was expected for a typical evening. However, $H_2O_{(g)}$ remained high over the course (~ 6 g kg^{-1}), suggestive of BL air masses. Indeed, the sampling site experienced relatively high pressure, temperature, and RH during this period, indicative of different synoptic conditions. In addition, nighttime $H_2O_{(g)}$ mixing ratios in August appeared to be higher than those in July in general (Fig. S14). This may also associate with synoptic weather. Based on these observations, we believe that $H_2O_{(g)}$ is a better criterion for differentiating FL and BL-influenced air masses than modeled BL height. We based on Zhang and Jaffe (2017) and classify periods with observed $H_2O_{(g)}$ above the minimum monthly water vapor criteria value, 2.5 g kg^{-1}, and CO > 80 ppb as those dominated by "BL-influenced air" and the rest by "FT air".

Table S1. A summary of mass concentration and composition of NR-PM_1 species measured at different high-altitude locations around the world

Location[1]	Altitude (m a.s.l.)	Sampling Time	Air mass type	Instrument[2]	NR-PM_1 ($\mu g\ m^{-3}$)	Mass fraction of NR-PM_1 (%)					Reference
						Org	SO_4	NO_3	NH_4	Chl	
MBO	2763	Jul. - Aug. 2013	Mixed	HR-AMS	3.16	85	11	1	3	0	this study
MBO	2763	Jul. - Aug. 2013	FT	HR-AMS	0.85	54	39	1	6	0	this study
NE Pac.	> 3000	May, 2006	FT	HR-AMS	0.7	27	53	2	18	0	Dunlea et al. (2009)
Whistler	2182	Apr. - May, 2006	Mixed	HR-AMS	1.9	55	30	3	12	0	Sun et al. (2009)
Sierra	1315	Aug. - Sept., 2007	BL	HR-AMS	4.1	73	15	5	7	0	Worton et al. (2011)
SPL	3210	Apr., 2004	Mixed	Q-AMS	2.11	42	28	10	19	1	Zhang et al. (2007)
RMNP	2740	Aug., 2010	Mixed	HR-AMS	5.13	75	17	4	4	0	Schurman et al. (2015)
WF. Mt.	600	Jul. -Aug., 2002	Mixed	Q-AMS	1.41	67	27	2	4	0	Zhang et al. (2007)
PdD	1450	Summer, 2010	Mixed	C-AMS	21.7	57	20	9	14	0	Freney et al. (2011)
PdD	1450	Feb. 2012	FT	C-AMS	-	42	45	5	8	0	Freney et al. (2016)
JFJ	3580	Summer, 2013	Mixed	ACSM	0.8	57	22	8	13	0	Fröhlich et al. (2015)
JFJ	3580	Jul. 2012 - Oct. 2013	FT	ACSM	0.5	42	44	4	10	0	Fröhlich et al. (2015)
Mt. CM	2165	Jun. - Jul., 2012	Mixed	HR-AMS	4.5	63	21	7	9	0	Rinaldi et al. (2015)
Nam Co	4730	Jun. - Jul., 2015	Mixed	HR-AMS	1.84	74	16	2	8	0	Xu et al. (2018)
Mt. WZ	958	Mar. - Apr., 2015	mixed	HR-AMS	10.2	47	33	5	15	0	Zhu et al. (2016)
E. Asia	1-3 km	Mar. - May, 2001	mixed	Q-AMS	7.8	45	59	7	19	0	Bahreini et al. (2003)

[1]Locations:

MBO: Mt. Bachelor Observatory, OR, USA
NE Pac.: Northeast Pacific
Whistler: Whistler Mountain, Canada

Sierra: Sierra Nevada, USA
SPL: Storm Peak Laboratory, USA
RMNP: Rocky Mountains National Park, USA
WF. Mt.: Whiteface Mountain, USA
PdD: Puy-de-Dome, France
JFJ: Jungfraujoch, Swizerland
Mt. CM: Mt. Cimone, Italy
Tibet: Tibet, China
Mt. WZ: Mt. Wuzhi, China
E. Asia: East Asia

[2]Instruments:

HR-AMS: High Resolution Time-of-Flight Aerosol Mass Spectrometer
Q-AMS: Quardropule Aerosol Mass Spectrometer
C-AMS: Compact Time-of-Flight Aerosol Mass Spectrometer
ACSM: Aerosol Chemical Speciation Monitor

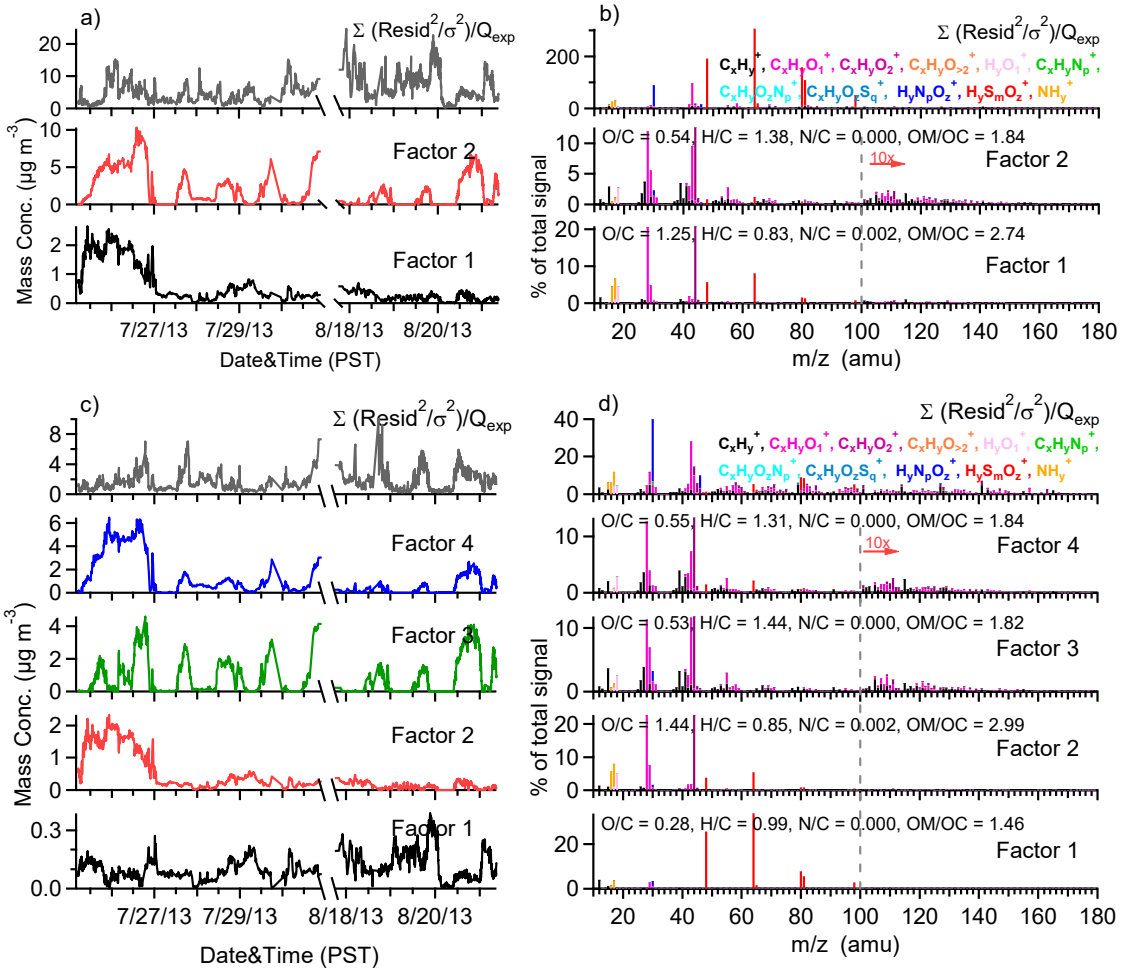

Fig. S1. Time series and mass spectral profiles of total Q/Q_{exp} and each OA factor for the 2-factor (a, b) and 4-factor (c, d) solution.

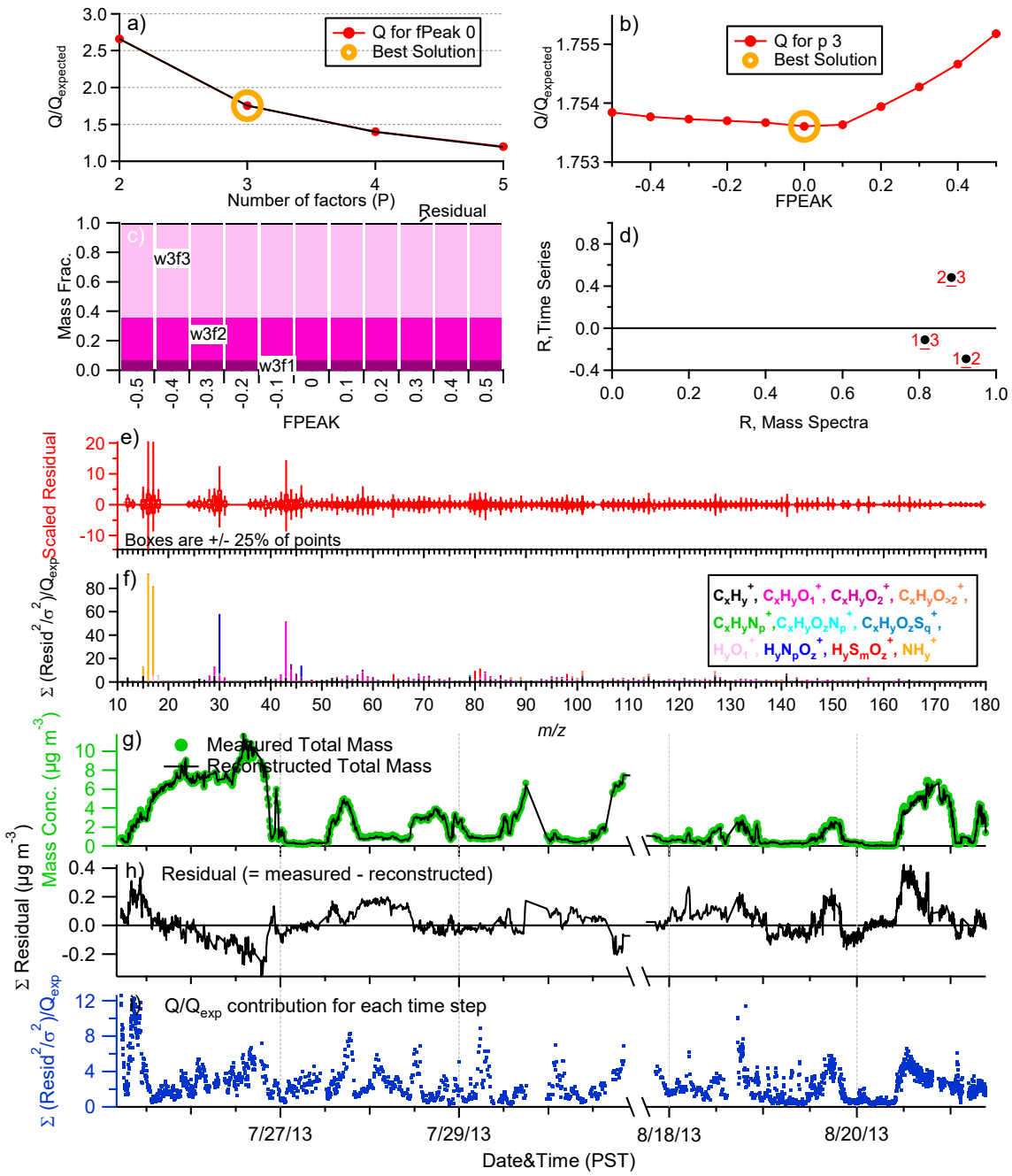

Fig. S2. Summary of the evaluation of PMF results for the 3-factor solution: (a) Q/Q_{exp} as a function of number of factors (P), (b) Q/Q_{exp} as a function of fPeak values, (c) fractions of PMF factors as a function of fPeak values, (d) correlations among the 3 factors in terms of mass spectrum and time series, (e) box plot of the scaled residuals for each ion, (f) Q/Q_{exp} values for each ion, (g) time series of the measured and reconstructed NR-PM_1 mass concentration, (h) residual time series, and (i) Q/Q_{exp} time series.

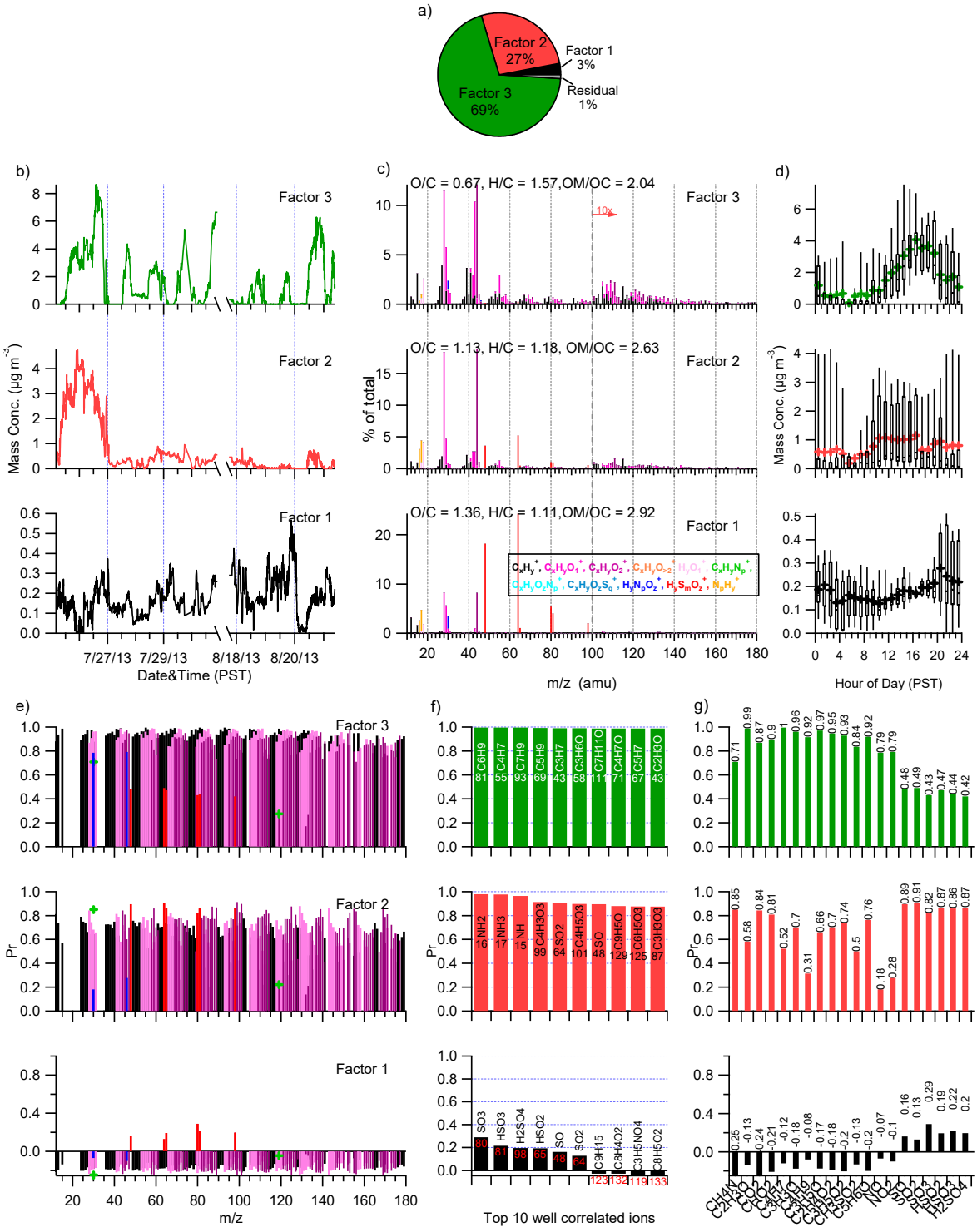

Fig. S3. PMF results for the 3-factor solution: (a) time series, (b) high-resolution mass spectrum (HRMS) colored by eight ion families, and (c) diurnal variations of each factor. The elemental ratios (IA method) of each OA factor are shown in the legends of (c). Correlations (Pearson's r) between each OA factor and (e) the HRMS ions (share color code in (c)), (f) top 10 HRMS ions that showed the tightest correlation, and (g) characteristic ions. The nominal

mass and identity of the top 10 HRMS ions are shown in (f). The Pearson's r number between each OA factor and the characteristic ions are shown in (g).

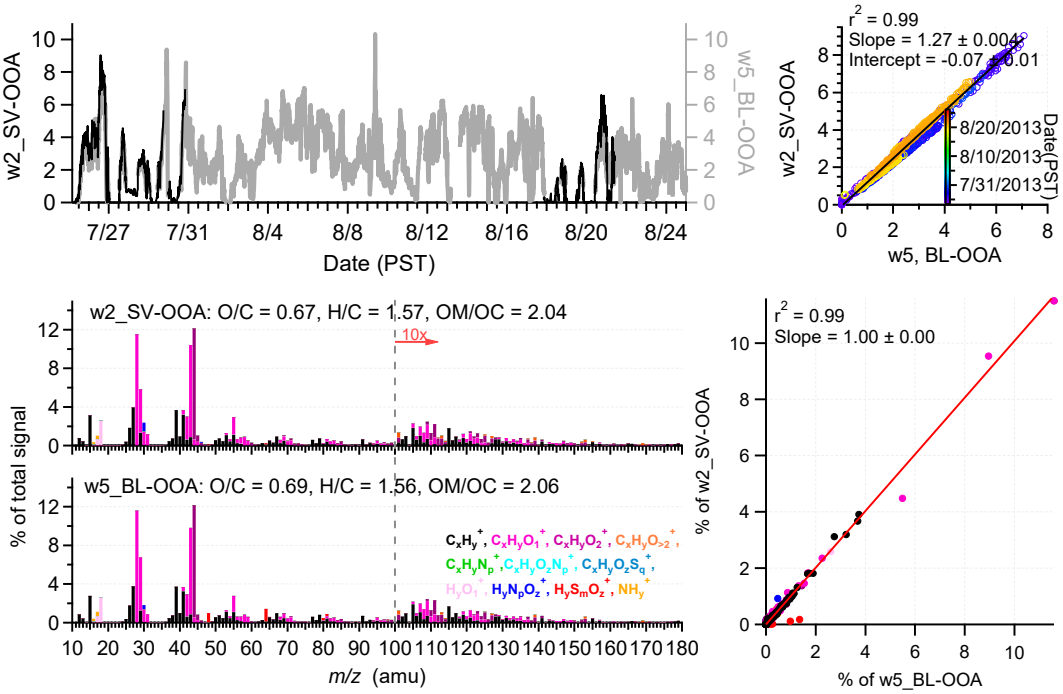

Fig. S4. Comparison of the time series (upper panel) and mass spectrum (lower panels) between the SV-OOA factor in the reconstructed 2-factor solution determined in this study (w2_BL-OOA) and the BL-OOA factor from the 5-factor solution determined in Zhou et al. (2017) (w5_BL-OOA).

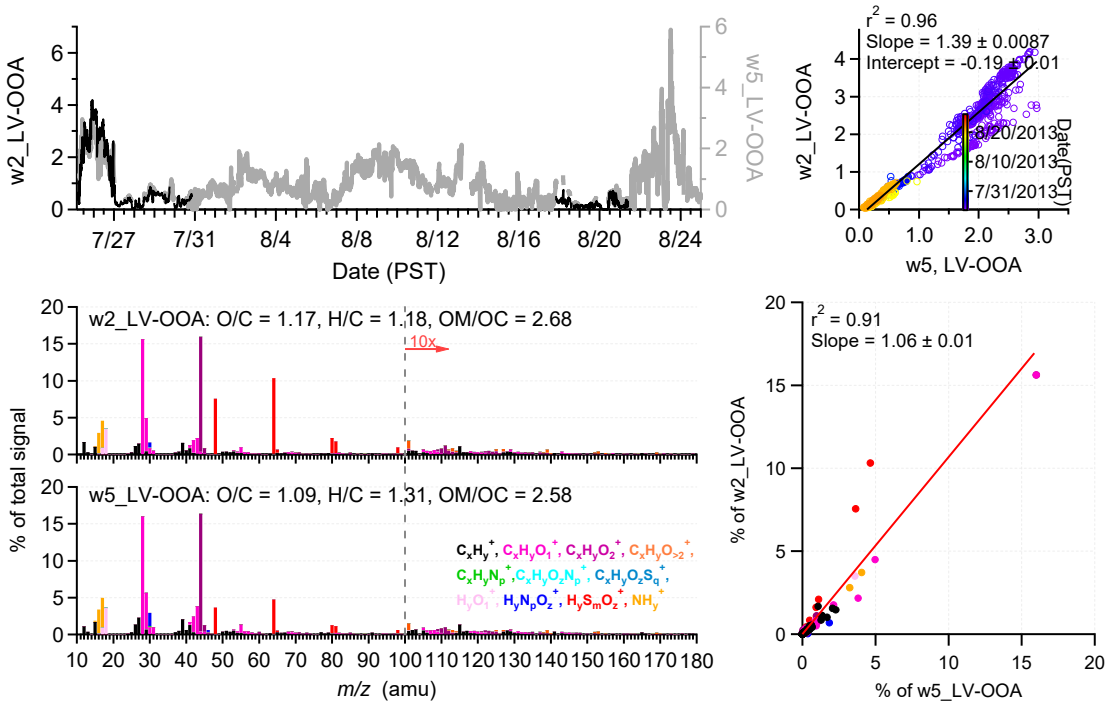

Fig. S5. Comparison of the time series (upper panel) and mass spectrum (lower panel) between the LV-OOA factor in the reconstructed 2-factor solution determined in this study (w2_FT-OOA) and the LV-OOA factor from the 5-factor solution determined in Zhou et al. (2017) (w5_LV-OOA).

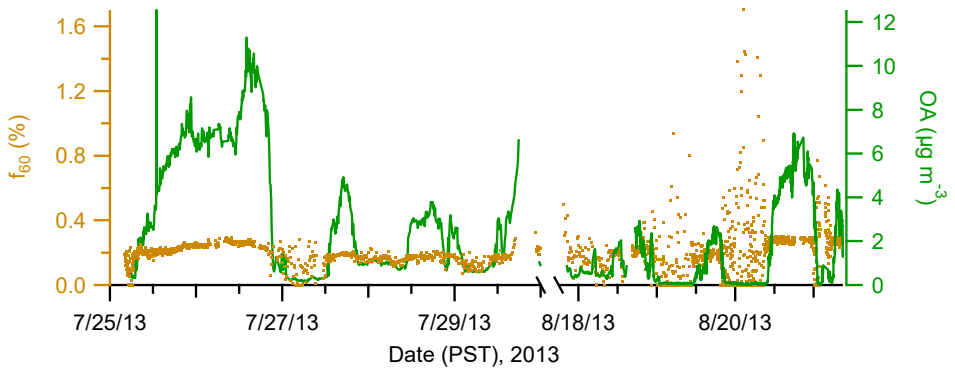

Fig. S6. Time series of f_{60}, the fraction of $C_2H_4O_2^+$ (m/z = 60.021) signal over total OA, and total OA mass concentration during the clean periods.

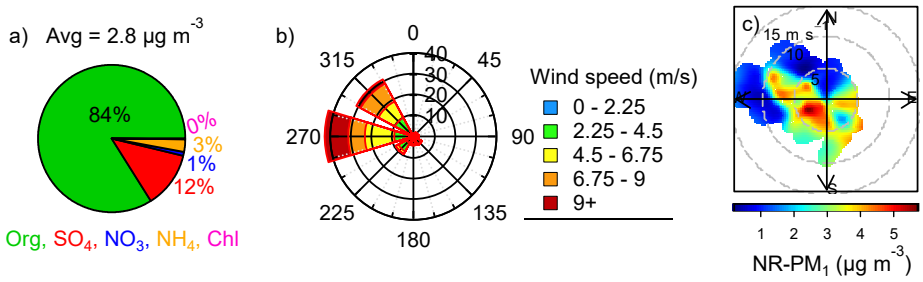

Fig. S7. Average (a) NR-PM_1 composition, (b) wind rose, and (c) bivariate polar plots of NR-PM_1 concentrations during the clean periods.

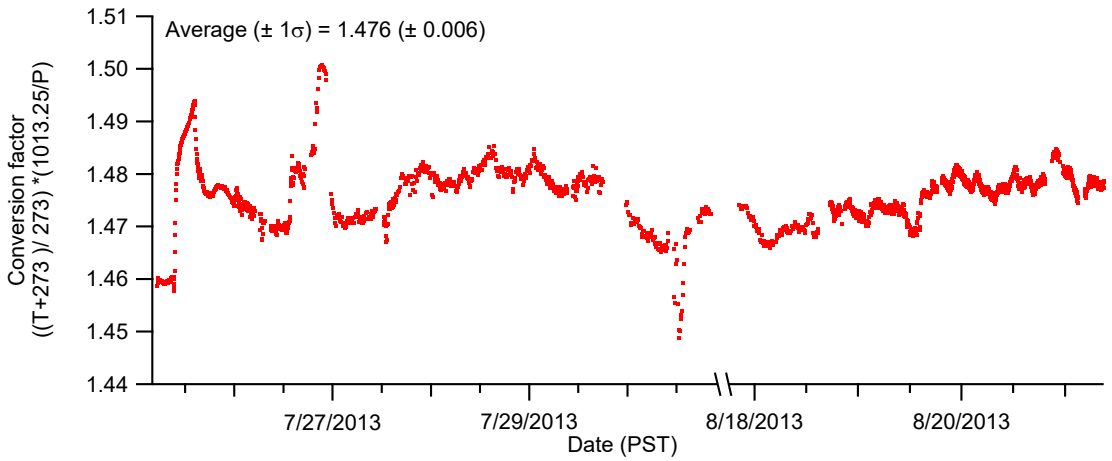

Fig. S8. Time series of the factor converting aerosol mass concentration under ambient temperature and pressure at MBO to that under standard temperature (K = 273 K) and pressure (P = 1013.25 hPa).

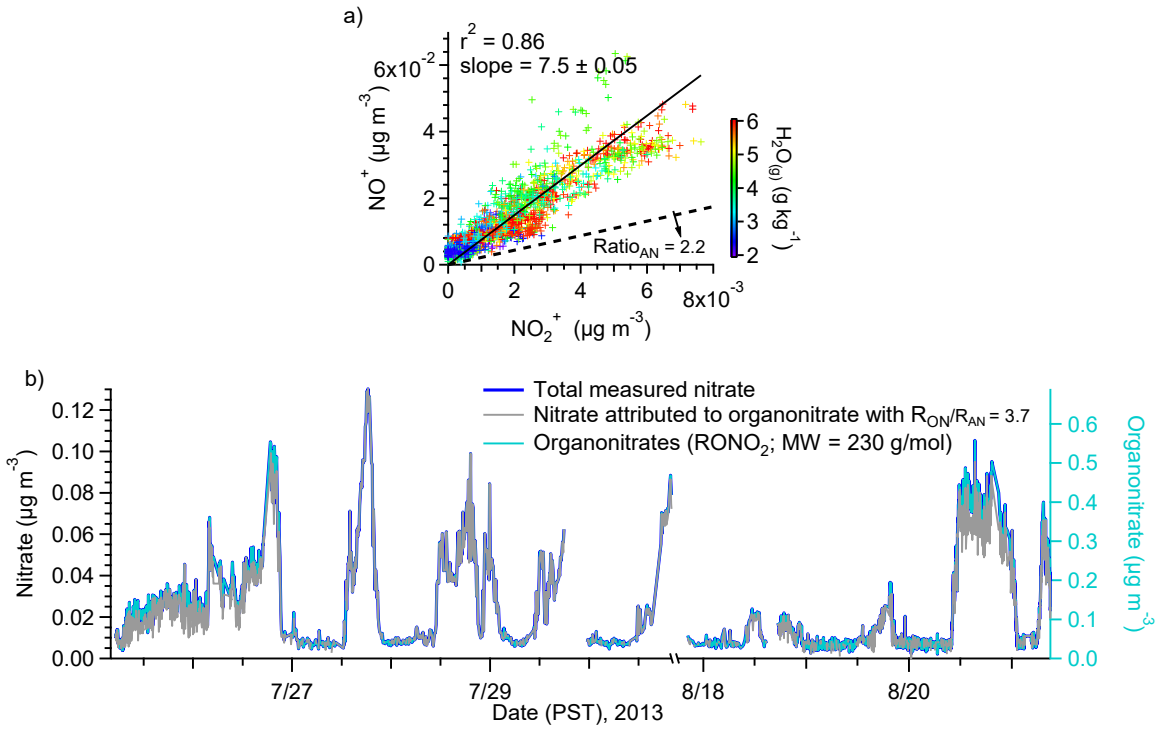

Fig. S9. (a) Scatter plot of NO^+ vs. NO_2^+ colored by water vapor mixing ratio. Data fitting was performed using the orthogonal distance regression (ODR) forced through origin. (b) Time series of total measured nitrate and estimated nitrate attributed to organonitrates on the left axis, and estimated organonitrate mass concentration on the right axis.

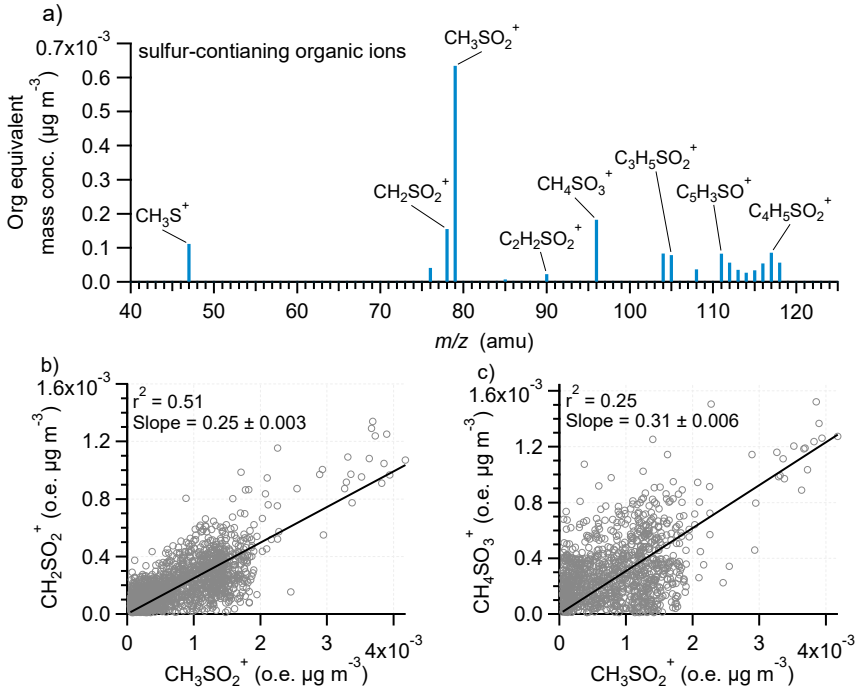

Fig. S10. (a) Average high-resolution aerosol mass spectrum of the organosulfur ions detected at MBO. Scatter plots of (b) $CH_2SO_2^+$ and (c) $CH_4SO_3^+$ vs. $CH_3SO_2^+$ in organic-equivalent mass concentration. Data fitting was performed using the orthogonal distance regression (ODR) forced through origin.

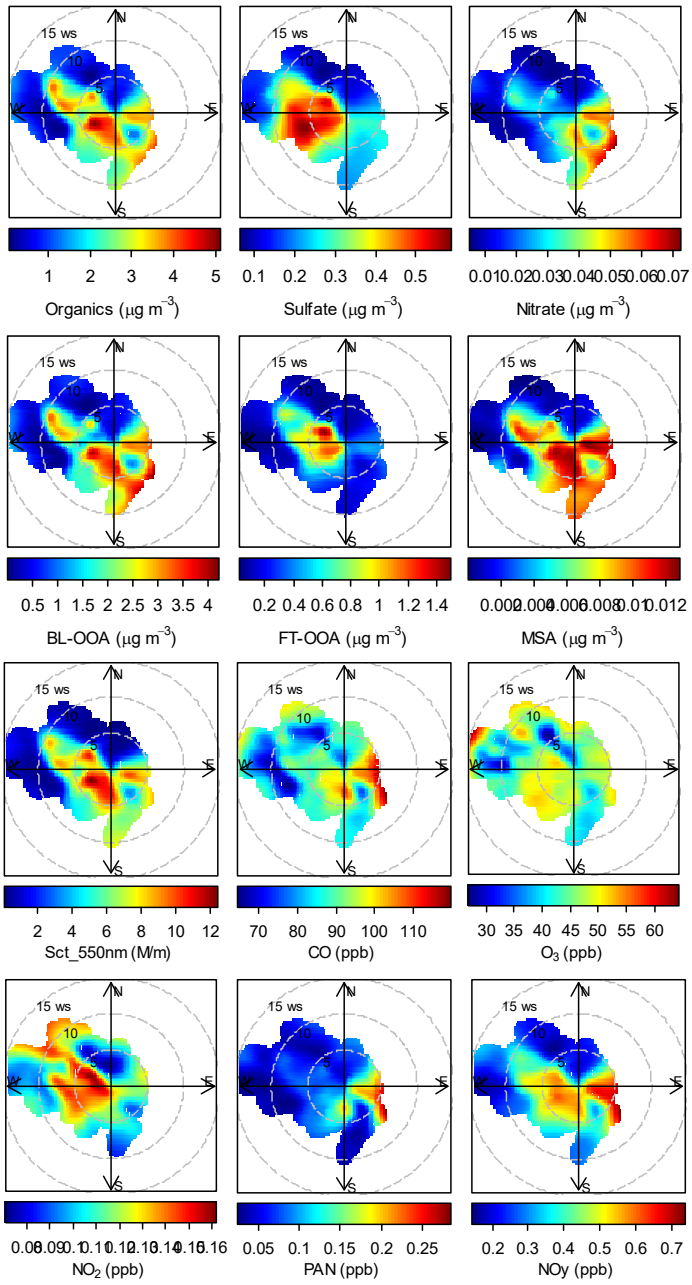

Fig. S11. Bivariate polar plots of aerosol and gas species measured at MBO during the clean periods.

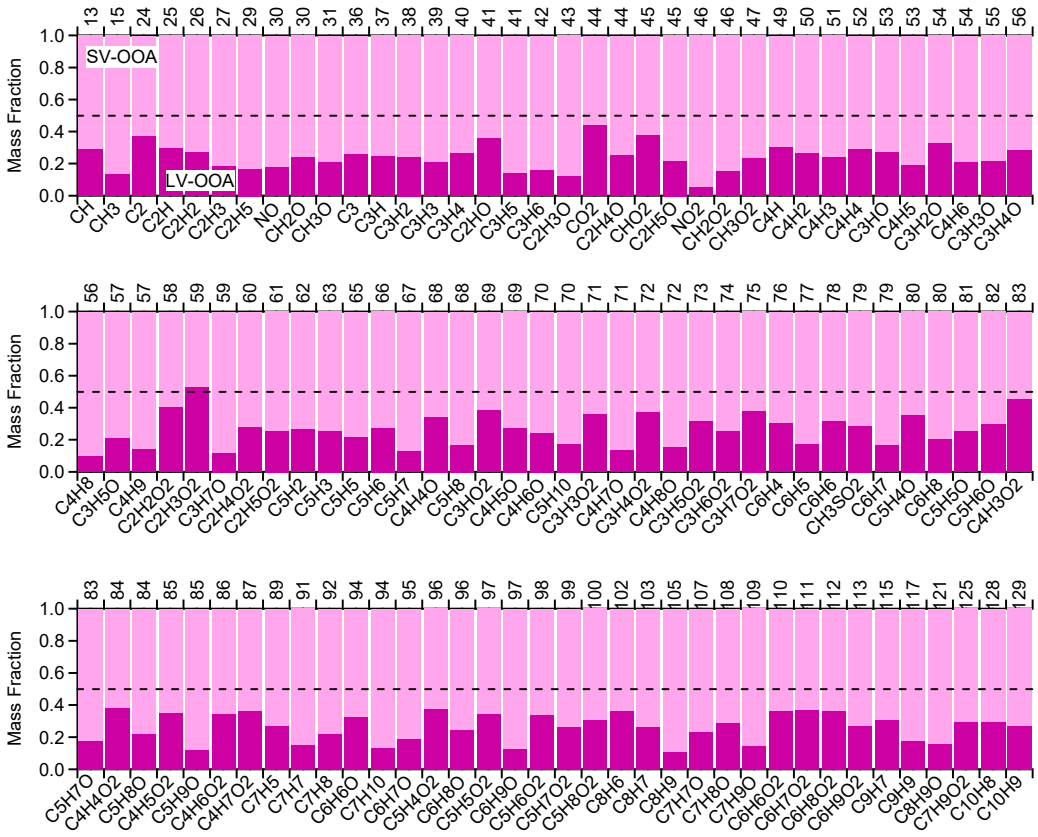

Fig. S12. Ion signal distribution between two PMF factors for additional ions that were not presented in Fig.4. Nominal masses of individual ions are shown on the top axes.

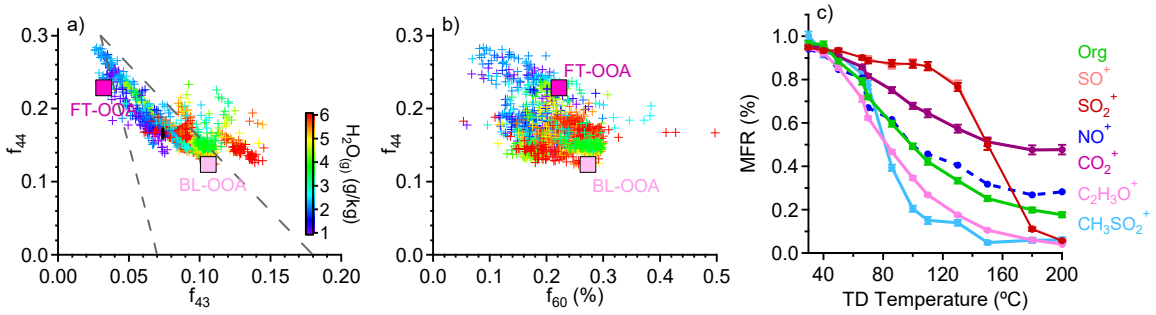

Fig. S13. (a) f_{44} versus f_{43} (b) f_{44} versus f_{60} for extracted OA factors (square) and the measured ambient OA during the clean periods colored by water vapor mixing ratio (cross). The black dashed lines in (a) show the boundaries set by (Ng et al., 2010). (c) Mass fraction remaining (MFR) of total organics and selected signature ions as a function of thermodenuder (TD) temperature during the clean periods.

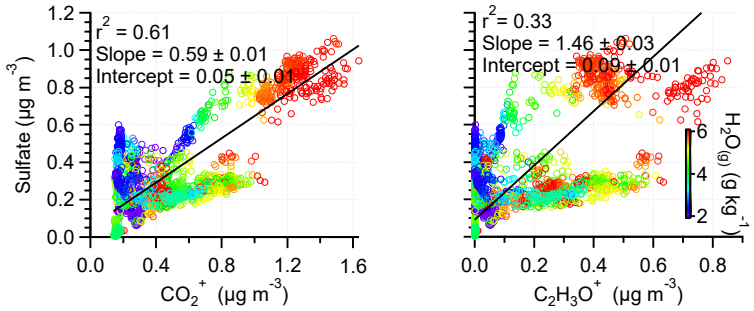

Fig. S14. Scatter plots of sulfate vs. CO_2^+ and $C_2H_3O^+$ colored by water vapor mixing ratio. Data fitting was performed using the orthogonal distance regression (ODR). CO_2^+ and $C_2H_3O^+$ are in organic-equivalent mass concentration.

References

Ambrose, J. L., Reidmiller, D. R., and Jaffe, D. A.: Causes of high O3 in the lower free troposphere over the Pacific Northwest as observed at the Mt. Bachelor Observatory, Atmos. Environ., 45, 5302-5315, 2011.

Bahreini, R., Jimenez, J. L., Wang, J., Flagan, R. C., Seinfeld, J. H., Jayne, J. T., and Worsnop, D. R.: Aircraft-based aerosol size and composition measurements during ACE-Asia using an Aerodyne aerosol mass spectrometer, J. Geophys. Res. Atmos.,, 108, 8645, 2003.

Collaud Coen, M., Weingartner, E., Furger, M., Nyeki, S., Prévôt, A. S. H., Steinbacher, M., and Baltensperger, U.: Aerosol climatology and planetary boundary influence at the Jungfraujoch analyzed by synoptic weather types, Atmos. Chem. Phys., 11, 5931-5944, 2011.

Dunlea, E. J., DeCarlo, P. F., Aiken, A. C., Kimmel, J. R., Peltier, R. E., Weber, R. J., Tomlinson, J., Collins, D. R., Shinozuka, Y., McNaughton, C. S., Howell, S. G., Clarke, A. D., Emmons, L. K., Apel, E. C., Pfister, G. G., van Donkelaar, A., Martin, R. V., Millet, D. B., Heald, C. L., and Jimenez, J. L.: Evolution of Asian aerosols during transpacific transport in INTEX-B, Atmos. Chem. Phys., 9, 7257-7287, 2009.

Fischer, E. V., Jaffe, D. A., Reidmiller, D. R., and Jaegle, L.: Meteorological controls on observed peroxyacetyl nitrate at Mount Bachelor during the spring of 2008, J. Geophys. Res. Atmos.,, 115, 2010.

Freney, E., Sellegri, K., Asmi, E., Rose, C., Chauvigne, A., Baray, J. L., Colomb, A., Hervo, M., Montoux, N., Bouvier, L., and Picard, D.: Experimental Evidence of the Feeding of the Free Troposphere with Aerosol Particles from the Mixing Layer, Aerosol Air Qual. Res., 16, 702-716, 2016.

Freney, E. J., Sellegri, K., Canonaco, F., Boulon, J., Hervo, M., Weigel, R., Pichon, J. M., Colomb, A., Prévôt, A. S. H., and Laj, P.: Seasonal variations in aerosol particle composition at the puy-de-Dôme research station in France, Atmos. Chem. Phys., 11, 13047-13059, 2011.

Fröhlich, R., Cubison, M. J., Slowik, J. G., Bukowiecki, N., Canonaco, F., Croteau, P. L., Gysel, M., Henne, S., Herrmann, E., Jayne, J. T., Steinbacher, M., Worsnop, D. R., Baltensperger, U., and Prévôt, A. S. H.: Fourteen months of on-line measurements of the non-refractory submicron aerosol at the Jungfraujoch (3580 m a.s.l.) – chemical composition, origins and organic aerosol sources, Atmos. Chem. Phys., 15, 11373-11398, 2015.

McClure, C. D., Jaffe, D. A., and Gao, H.: Carbon Dioxide in the Free Troposphere and Boundary Layer at the Mt. Bachelor Observatory, Aerosol Air Qual. Res., 16, 717-728, 2016.

Ng, N. L., Canagaratna, M. R., Zhang, Q., Jimenez, J. L., Tian, J., Ulbrich, I. M., Kroll, J. H., Docherty, K. S., Chhabra, P. S., Bahreini, R., Murphy, S. M., Seinfeld, J. H., Hildebrandt, L., Donahue, N. M., DeCarlo, P. F., Lanz, V. A., Prevot, A. S. H., Dinar, E., Rudich, Y., and Worsnop, D. R.: Organic aerosol components observed in Northern Hemispheric datasets from Aerosol Mass Spectrometry, Atmos. Chem. Phys., 10, 4625-4641, 2010.

Reidmiller, D. R., Jaffe, D. A., Fischer, E. V., and Finley, B.: Nitrogen oxides in the boundary layer and free troposphere at the Mt. Bachelor Observatory, Atmos. Chem. Phys., 10, 6043-6062, 2010.

Rinaldi, M., Gilardoni, S., Paglione, M., Sandrini, S., Fuzzi, S., Massoli, P., Bonasoni, P., Cristofanelli, P., Marinoni, A., Poluzzi, V., and Decesari, S.: Organic aerosol evolution and transport observed at Mt. Cimone (2165 m a.s.l.), Italy, during the PEGASOS campaign, Atmos. Chem. Phys., 15, 11327-11340, 2015.

Schurman, M. I., Lee, T., Sun, Y., Schichtel, B. A., Kreidenweis, S. M., and Collett Jr, J. L.: Investigating types and sources of organic aerosol in Rocky Mountain National Park using aerosol mass spectrometry, Atmos. Chem. Phys., 15, 737-752, 2015.

Sun, Y., Zhang, Q., Macdonald, A. M., Hayden, K., Li, S. M., Liggio, J., Liu, P. S. K., Anlauf, K. G., Leaitch, W. R., Steffen, A., Cubison, M., Worsnop, D. R., van Donkelaar, A., and Martin, R. V.: Size-resolved aerosol chemistry on Whistler Mountain, Canada with a high-resolution aerosol mass spectrometer during INTEX-B, Atmos. Chem. Phys., 9, 3095-3111, 2009.

Venzac, H., Sellegri, K., Villani, P., Picard, D., and Laj, P.: Seasonal variation of aerosol size distributions in the free troposphere and residual layer at the puy de Dome station, France, Atmospheric Chemistry and Physics, 9, 1465-1478, 2009.

Weiss-Penzias, P., Jaffe, D. A., Swartzendruber, P., Dennison, J. B., Chand, D., Hafner, W., and Prestbo, E.: Observations of Asian air pollution in the free troposphere at Mount Bachelor Observatory during the spring of 2004, J. Geophys. Res. Atmos.,, 111, D10304, 2006.

Worton, D. R., Goldstein, A. H., Farmer, D. K., Docherty, K. S., Jimenez, J. L., Gilman, J. B., Kuster, W. C., de Gouw, J., Williams, B. J., Kreisberg, N. M., Hering, S. V., Bench, G., McKay, M., Kristensen, K., Glasius, M., Surratt, J. D., and Seinfeld, J. H.: Origins and composition of fine atmospheric carbonaceous aerosol in the Sierra Nevada Mountains, California, Atmos. Chem. Phys., 11, 10219-10241, 2011.

Xu, J., Zhang, Q., Shi, J., Ge, X., Xie, C., Wang, J., Kang, S., Zhang, R., and Wang, Y.: Chemical characteristics of submicron particles at the central Tibetan Plateau: insights from aerosol mass spectrometry, Atmos. Chem. Phys., 18, 427-443, 2018.

Zhang, L. and Jaffe, D. A.: Trends and sources of ozone and sub-micron aerosols at the Mt. Bachelor Observatory (MBO) during 2004–2015, Atmos. Environ., 165, 143-154, 2017.

Zhang, Q., Jimenez, J. L., Canagaratna, M. R., Allan, J. D., Coe, H., Ulbrich, I., Alfarra, M. R., Takami, A., Middlebrook, A. M., Sun, Y. L., Dzepina, K., Dunlea, E., Docherty, K., DeCarlo, P. F., Salcedo, D., Onasch, T., Jayne, J. T., Miyoshi, T., Shimono, A., Hatakeyama, S., Takegawa, N., Kondo, Y., Schneider, J., Drewnick, F., Borrmann, S., Weimer, S., Demerjian, K., Williams, P., Bower, K., Bahreini, R., Cottrell, L., Griffin, R. J., Rautiainen, J., Sun, J. Y., Zhang, Y. M., and Worsnop, D. R.: Ubiquity and dominance of oxygenated species in organic aerosols in anthropogenically-influenced Northern Hemisphere midlatitudes, Geophys Res Lett, 34, 6, 2007.

Zhou, S., Collier, S., Jaffe, D. A., Briggs, N. L., Hee, J., Sedlacek Iii, A. J., Kleinman, L., Onasch, T. B., and Zhang, Q.: Regional influence of wildfires on aerosol chemistry in the western US and insights into atmospheric aging of biomass burning organic aerosol, Atmos. Chem. Phys., 17, 2477-2493, 2017.

Zhu, Q., He, L. Y., Huang, X. F., Cao, L. M., Gong, Z. H., Wang, C., Zhuang, X., and Hu, M.: Atmospheric aerosol compositions and sources at two national background sites in northern and southern China, Atmos. Chem. Phys., 16, 10283-10297, 2016.